Chapter 1

Numerical Modeling of Nonlinear Surface Waves and Its Validation

Wooyoung Choi, Christopher P. Kent and Caleb J. Schillinger
Department of Naval Architecture & Marine Engineering
University of Michigan, Ann Arbor, MI 48109

We study numerically the evolution of nonlinear surface gravity waves in infinitely deep water using both the exact evolution equations and an asymptotic model correct to the third order in wave steepness. For one-dimensional Stokes waves subject to perturbations at sideband frequencies, the numerical solutions of the third-order nonlinear model found using a pseudo-spectral method are carefully validated with those of the exact equations, and it is found that the third-order model describes accurately the development of spectral components in time. For two-dimensional waves, we study resonant interactions of two mutually-orthogonal gravity wave trains and compare our numerical solutions with available theory and experimental data. We also simulate the evolution of a realistic surface wave field, characterized initially by the JONSWAP spectrum, and examine the occurrence of a larger wave compared with the background wave field.

1.1 Introduction

Accurate prediction of nonlinear surface wave fields is important to many engineering applications in both coastal and deep oceans. Recently, much attention has been paid to rogue waves, which often give rise to wave heights much greater than the significant wave height of a given spectrum. The occurrence of these intermittent waves is actively being investigated, but it is not yet well understood.

In order to describe such waves, fully nonlinear computations of sur-

face waves are desirable, but even with an idealized potential flow assumption, solving the three-dimensional free surface hydrodynamic equations is still computationally problematic. Therefore, simpler mathematical models have to be adopted for practical applications, but such models have been developed mainly for long waves in the shallow water regime (see Wu 1998, 2001 for a more recent development for dispersive nonlinear long waves).

Despite significant advances in the understanding of nonlinear wave interaction and wave instability in the 1960's, progress in numerical modeling of deep water waves, on the other hand, is relatively slow. Although the wave action approach for slowly varying wave fields is somewhat successful, the description of nonlinear interaction of different wave components mostly relies on the integral formulation proposed by Hasselmann (1962) and Zakharov (1968). The complexity of its formulation in the spectral space nevertheless keeps the formulation from being used in operational wave prediction models.

A much more effective formulation to study the evolution of nonlinear surface waves in infinitely deep water was first proposed by West *et al.* (1987). By expressing the solution of the Laplace equation via an integral operator and expanding the free surface boundary conditions about the mean free surface, they derived a closed system of nonlinear evolution equations in infinite series. Similar approaches have been also used in Matsuno (1992), Craig & Sulem (1993), Choi (1995), Smith (1998), and Choi & Kent (2004) to derive more general evolution equations that include the effects of finite water depth, bottom topography, and wave-body interaction. Although the system written in infinite series is valid for arbitrary wave steepness, the series has to be truncated for numerical computations, depending on the desired accuracy and computational efficiency.

In this paper, we consider a truncated model correct to the third order in wave steepness and examine its validity by comparing numerical solutions of the third-order model with fully nonlinear solutions of the Euler equations and with available experimental data. To find fully nonlinear solutions for the two-dimensional Euler equations, we use the system of exact evolution equations first derived by Ovsjannikov (1974) using an unsteady conformal mapping method (see also Dyachenko, Zakharov & Kuznetsov 1996; Choi & Camassa 1999). To solve both the exact and the third-order systems numerically, we adopt a pseudo-spectral method based on Fourier series, as described in Kent & Choi (2004).

Three different numerical experiments are described. First, one-dimensional progressive waves subject to perturbations at sideband frequencies are chosen to test the third-order model and the time evolution of spectral components is carefully examined. Secondly, we study nonlinear resonant interaction among two primary wave trains propagating in

mutually perpendicular directions. It has been known that resonant interactions can occur at third order so that a mode not initially present may be excited by the nonlinear interaction between two existing modes (Phillips 1960; Longuet-Higgins 1962). We numerically reproduce the experiments of McGoldrick *et al.* (1966) and compare our numerical solutions with their observations. Lastly, we present the evolution of a more realistic random, directional, oceanic sea state characterized initially by the JONSWAP spectrum with directional spreading.

1.2 Mathematical Formulation

On the free surface of an ideal fluid, the boundary conditions can be written, in terms of the surface elevation $\zeta(x, y, t)$ and the free surface velocity potential $\Phi(x, y, t) \equiv \varphi(x, y, \zeta, t)$ (Zakharov 1968), as

$$\frac{\partial \zeta}{\partial t} + \boldsymbol{\nabla}\Phi\cdot\boldsymbol{\nabla}\zeta = \left(1 + |\boldsymbol{\nabla}\zeta|^2\right) W\,, \tag{1.1}$$

$$\frac{\partial \Phi}{\partial t} + \tfrac{1}{2}|\boldsymbol{\nabla}\Phi|^2 + g\zeta = \tfrac{1}{2}\left(1 + |\boldsymbol{\nabla}\zeta|^2\right) W^2\,, \tag{1.2}$$

where $\varphi(x, y, z, t)$ is the three-dimensional velocity potential, g is the gravitational acceleration, $\boldsymbol{\nabla}$ is the horizontal gradient defined by $\boldsymbol{\nabla} = (\partial/\partial x, \partial/\partial y)$, and W is the vertical velocity evaluated at the free surface, $W \equiv \left.\frac{\partial\varphi}{\partial z}\right|_{z=\zeta}$.

1.2.1 *Asymptotic expansion*

By expanding the free surface velocity potential about the mean free surface and using a property of harmonic functions, it has been shown (West *et al.* 1987; Choi 1995; Kent & Choi 2004) that the vertical velocity at the free surface, W, can be expanded as

$$W = \sum_{n=1}^{\infty} W_n, \qquad W_n = \sum_{j=1}^{n} C_{n-j}\Big[\varphi_j\Big], \tag{1.3}$$

where $W_n = O(\epsilon^n)$ with ϵ being the wave slope defined by ϵ=wave amplitude/wave length, and $\varphi_j = O(\epsilon^j)$ can be found recursively, as a function of ζ and Φ, from

$$\varphi_1(x, y, t) = \Phi(x, y, t), \qquad \varphi_j(x, y, t) = -\sum_{l=1}^{j-1} \mathcal{A}_{j-l}[\varphi_l] \quad \text{for } j \geq 2. \tag{1.4}$$

In (1.3)-(1.4), two operators $\mathcal{A}_n$ and $\mathcal{C}_n$ are defined, for even $n = 2m$ $(m = 0, 1, 2, \cdots)$, by

$$\mathcal{A}_{2m} = (-1)^m \frac{\zeta^{2m}}{(2m)!} \triangle^m, \quad \mathcal{C}_{2m} = (-1)^{m+1} \frac{\zeta^{2m}}{(2m)!} \triangle^m \mathcal{L}, \tag{1.5}$$

and, for odd $n = 2m + 1$ $(m = 0, 1, 2, \cdots)$, by

$$\mathcal{A}_{2m+1} = (-1)^{m+1} \frac{\zeta^{2m+1}}{(2m+1)!} \triangle^m \mathcal{L}, \quad \mathcal{C}_{2m+1} = (-1)^{m+1} \frac{\zeta^{2m+1}}{(2m+1)!} \triangle^{m+1}, \tag{1.6}$$

where the linear integral operator $\mathcal{L}$ is defined by

$$\mathcal{L}\left[\varphi_j\right] = \frac{1}{2\pi} \int \int_{-\infty}^{\infty} \frac{(\boldsymbol{x}' - \boldsymbol{x}) \cdot \boldsymbol{\nabla} \varphi_j}{|\boldsymbol{x}' - \boldsymbol{x}|^3} \, \mathrm{d}x' \mathrm{d}y'. \tag{1.7}$$

1.2.2 *Nonlinear evolution equations*

Since φ_j, and therefore W, are functions of ζ and Φ, by substituting (1.3) for W into (1.1)–(1.2), we have a closed system of nonlinear evolution equations for ζ and Φ in the form of:

$$\frac{\partial \zeta}{\partial t} = \sum_{n=1}^{\infty} \mathrm{Q}_n(\zeta, \Phi), \qquad \frac{\partial \Phi}{\partial t} = \sum_{n=1}^{\infty} \mathrm{R}_n(\zeta, \Phi). \tag{1.8}$$

In (1.8), Q_n and R_n representing the terms of $O(\epsilon^n)$ are given by

$$\begin{aligned} &\mathrm{Q}_1 = W_1, \quad \mathrm{Q}_2 = -\boldsymbol{\nabla}\Phi \cdot \boldsymbol{\nabla}\zeta + W_2, \\ &\mathrm{Q}_n = W_n + |\boldsymbol{\nabla}\zeta|^2 W_{n-1} \quad \text{for } n \geq 3, \end{aligned} \tag{1.9}$$

$$\begin{aligned} &\mathrm{R}_1 = -g\zeta, \quad \mathrm{R}_2 = -\tfrac{1}{2}|\boldsymbol{\nabla}\Phi|^2 + \tfrac{1}{2}{W_1}^2, \quad \mathrm{R}_3 = W_1 \, W_2, \\ &\mathrm{R}_n = \tfrac{1}{2} \sum_{j=0}^{n-2} W_{n-j-1} \, W_{j+1} \\ &\qquad + \tfrac{1}{2}|\boldsymbol{\nabla}\zeta|^2 \sum_{j=0}^{n-4} W_{n-j-3} \, W_{j+1} \quad \text{for } n \geq 4. \end{aligned} \tag{1.10}$$

Although the system valid to arbitrary order can be found from (1.8)–

(1.10), we consider the third-order system correct to $O(\epsilon^3)$:

$$\frac{\partial\zeta}{\partial t} + \mathcal{L}[\Phi] + \boldsymbol{\nabla}\cdot(\zeta\boldsymbol{\nabla}\Phi) + \mathcal{L}\Big[\zeta\mathcal{L}[\Phi]\Big] + \nabla^2\left(\tfrac{1}{2}\zeta^2\mathcal{L}[\Phi]\right) + \mathcal{L}\left[\zeta\mathcal{L}\Big[\zeta\mathcal{L}[\Phi]\Big] + \tfrac{1}{2}\zeta^2\nabla^2\Phi\right] = 0, \quad (1.11)$$

$$\frac{\partial\Phi}{\partial t} + g\zeta + \tfrac{1}{2}\boldsymbol{\nabla}\Phi\cdot\boldsymbol{\nabla}\Phi - \tfrac{1}{2}(\mathcal{L}[\Phi])^2 - \mathcal{L}[\Phi]\left(\zeta\nabla^2\Phi + \mathcal{L}\Big[\zeta\mathcal{L}[\Phi]\Big]\right) = 0, \quad (1.12)$$

and the numerical solutions of this system will be compared with the Euler solutions.

1.2.3 *Pseudo-spectral method*

To solve the system (1.11)–(1.12) numerically, the surface elevation ζ and the free surface velocity potential Φ are represented by the double Fourier series:

$$\zeta(\boldsymbol{x},t) = \sum_{n=-\frac{N}{2}}^{\frac{N}{2}} \sum_{m=-\frac{M}{2}}^{\frac{M}{2}} a_{nm}(t)\,\mathrm{e}^{inK_1x+imK_2y}, \quad (1.13)$$

$$\Phi(\boldsymbol{x},t) = \sum_{n=-\frac{N}{2}}^{\frac{N}{2}} \sum_{m=-\frac{M}{2}}^{\frac{M}{2}} b_{nm}(t)\,\mathrm{e}^{inK_1x+imK_2y}, \quad (1.14)$$

where N and M are the numbers of Fourier modes in the x- and y-directions, respectively, and $K_1 = 2\pi/L_1$ and $K_2 = 2\pi/L_2$ with L_1 and L_2 being the computational domain lengths in the x- and y-directions, respectively. When acting on a Fourier component, the integral operator $\mathcal{L}$ in (1.7) is defined by

$$\mathcal{L}\left[\mathrm{e}^{i\boldsymbol{k}\cdot\boldsymbol{x}}\right] = -k\,\mathrm{e}^{i\boldsymbol{k}\cdot\boldsymbol{x}}, \quad (1.15)$$

where $\boldsymbol{k} = (k_1, k_2)$ and $k = |\boldsymbol{k}|$, for which A_n and C_n in (1.5)–(1.6) can be simplified (West *et al.* 1987) to

$$\mathcal{A}_n = \frac{\zeta^n}{n!}\,k^n, \qquad \mathcal{C}_n = \frac{\zeta^n}{n!}\,k^{n+1}\,. \quad (1.16)$$

After evaluating the right-hand sides of (1.11)–(1.12) using a pseudo-spectral method (Fornberg & Whitham 1978), we integrate the evolution

equations using the fourth-order Runge-Kutta method. We check the accuracy of our numerical solutions by monitoring conservation of energy:

$$E = \tfrac{1}{2}\rho \iint \left\{ \Phi \sum_{n=1}^{\infty} \mathrm{Q}_n(\zeta, \Phi) + g\zeta^2 \right\} \mathrm{d}x\, \mathrm{d}y. \tag{1.17}$$

1.3 Validation of Models for One-dimensional Waves

1.3.1 *Exact evolution equations*

For a two-dimensional flow, using the conformal mapping technique, the evolution equations for the surface elevation $\eta(\xi, t) \equiv \zeta(\chi(\xi, t), t)$ and the velocity potential at the free surface $\phi(\xi, t) \equiv \Phi(\chi(\xi, t), t)$ parameterized in terms of ξ, can be found (Ovsjannikov 1974; Dyachenko *et al.* 1996) as

$$\begin{aligned} \frac{\partial \eta}{\partial t} &= -\chi_\xi \left(\frac{\psi_\xi}{J} \right) + \eta_\xi \, \mathcal{H} \left[\frac{\psi_\xi}{J} \right], \\ \frac{\partial \phi}{\partial t} &= -g\eta + \phi_\xi \, \mathcal{H} \left[\frac{\psi_\xi}{J} \right] - \frac{1}{2J} \left(\phi_\xi^2 - \psi_\xi^2 \right), \end{aligned} \tag{1.18}$$

where the subscript denotes differentiation with respect to ξ, the Hilbert transformation $\mathcal{H}$ is defined by

$$\mathcal{H}\big[\eta\big] = \fint_{-\infty}^{\infty} \frac{\eta(\xi', t)}{\xi' - \xi} \, \mathrm{d}\xi' \,, \tag{1.19}$$

and

$$J = {\chi_\xi}^2 + {\eta_\xi}^2. \tag{1.20}$$

In (1.18), $\chi(\xi, t)$ and $\psi(\xi, t)$ are the complex conjugates of $\eta(\xi, t)$ and $\phi(\xi, t)$, respectively, and can be found as

$$\chi_\xi = 1 - \mathcal{H}\Big[\eta_\xi\Big] \,, \qquad \psi_\xi = \mathcal{H}\Big[\phi_\xi - c\Big] \,, \tag{1.21}$$

where c is the velocity at infinity.

1.3.2 *Numerical method for exact evolution equations*

The system of exact evolution equations given by (1.18) are solved using a pseudo-spectral method similar to that for the third-order system. To reduce aliasing error, we add diffusive terms of $\nu D[\eta_{\xi\xi}]$ and $\nu D[\phi_{\xi\xi}]$ to the right-hand sides of (1.18), where constant ν is chosen to be $0.05\Delta\xi$ and D is a high-pass filter defined in the Fourier space which is 0 on the

lower 1/4 Fourier modes and 1 for the higher 1/4 modes; there is a linear transition between two regions. Therefore, there is no energy dissipation on the lower 1/4 modes. The detailed description of the method can be found in Yi, Hyman & Choi (2004). In order to make sure that no significant physical energy is dissipated by these *ad-hoc* terms, we carefully monitor conservation of total energy defined by

$$E = \int_{-L/2}^{L/2} \left(\phi_\xi \, \psi + g \, \eta^2 \chi_\xi \right) d\xi, \tag{1.22}$$

where L is the length of the total computational domain.

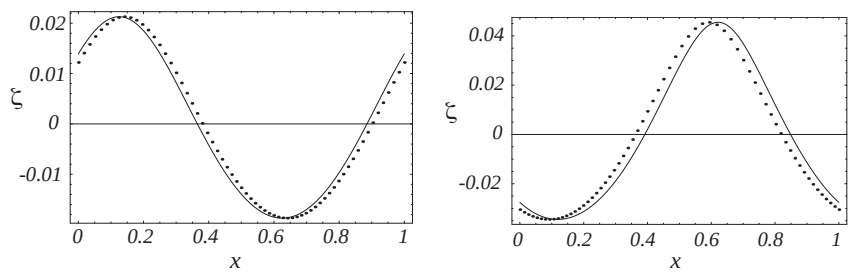

(a) (b)

Fig. 1.1 Progressive waves: Numerical solutions of the third-order model for ζ (—) compared with fully nonlinear solutions of the Euler equations $(\cdots)$ at $t = 50$ (approximately, 25 wave periods). (a) $a/\lambda = 0.02$, (b) $a/\lambda = 0.04$.

1.3.3 *Progressive waves*

For initial conditions, we choose the progressive wave solutions $(\zeta_p, \ \Phi_p)$ of the exact system (1.18) for amplitudes $a/\lambda = 0.02$ and $a/\lambda = 0.04$, found via the Newton-Raphson method (Choi & Camassa 1999), for both the third-order model (1.11)–(1.12) and the exact system (1.18). For these computations, to fix time and length scales, we choose $g = 1$ and $\lambda = 1$. Using $N = 128$ and Δt=0.001, a typical error in energy conservation is less than 0.001%. Two solutions at $t = 50$ (approximately, 25 wave periods) are compared in figure 1.1. Notice that there is a small error in phase velocity, but the wave profiles are well preserved for both wave amplitudes. For example, for the wave of $a = 0.04$, whose wave speed is $c \simeq 0.4117$, the error in amplitude is less than 0.01%, and the error in phase velocity is less than 0.2%. Therefore, the third-order model can be regarded as a good approximation to the Euler equations for these wave amplitudes. It is

interesting to notice that, compared with the exact solutions, the wave of the third-order model travels slightly slower for the smaller wave amplitude of $a = 0.02$, but faster for the larger wave amplitude of $a = 0.04$.

1.3.4 *Benjamin-Feir instability*

In order to validate the third-order model for time-dependent problems, we first consider the evolution of a progressive wave train subject to sideband perturbations which are known to be unstable (Benjamin & Feir 1967).

For initial conditions, the amplitude of the wave train is slightly modulated so that the free surface elevation ζ is given by

$$\zeta(x, 0) = \Big[1 + A\cos(Kx)\Big]\,\zeta_p(kx), \tag{1.23}$$

where $k = 2\pi/\lambda$ and $K = 2\pi/L$ are the wave numbers of the carrier wave and its envelope, respectively, and ζ_p represents the exact progressive wave solution of the Euler equations of wave amplitude a. Initially, no perturbation is added to the free surface velocity potential Φ_p. In our computations, $\lambda = 1$, $g = 1$, $a = 0.02$, $A = 0.1$, and $L = 8$. Notice that the wavelength of the wave envelope is the same as the length of the total computational domain. We use the total number of Fourier modes to be $N = 2^{10} = 1024$ ($2^7 = 128$ modes per wavelength, the same resolution as in the previous comparison for progressive waves) and $\Delta t = 0.001$. Again, the total energy is conserved to $O(10^{-3}\%)$ at $t = 240$ for both the third-order and the exact systems. Two solutions for wave profiles at different times are compared in figure 1.2, and they show excellent agreement in both wave amplitude and phase. Notice that the highest wave amplitude is more than twice the initial wave amplitude of the carrier wave. In figure 1.3, we also compare the wavenumber spectra defined by the amplitude of the complex Fourier coefficients. At $t = 0$, we can observe the first harmonic component of the carrier wave at $k/K = 8$ and small perturbations at two sideband wavenumbers of $k/K = 7$ and 9, as well as the higher harmonics of the carrier wave at $k/K = 16$ and $k/K = 24$. At the end of computation ($t = 240$), the spectrum becomes wider with the wave amplitude at the lower sideband mode being higher than that of the primary mode, as noted in the experiments of Lake *et al.* (1977). Except a small discrepancy in amplitude of the primary mode, the third-order system well captures the development of all spectral components.

As time increases, both systems continuously spread energy to higher harmonics and, therefore, the total energy in our computation starts to decrease at $t = 250$ due to our filter on higher harmonics to eliminate the aliasing error. It is well known that the nonlinear Schrödinger (NLS)

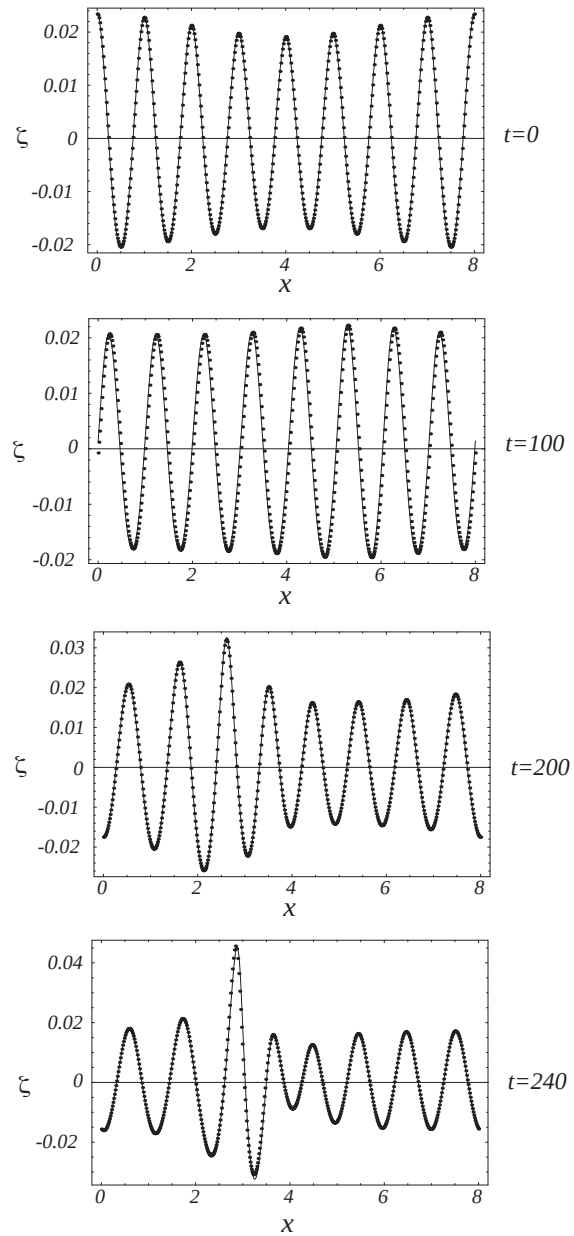

Fig. 1.2 Benjamin-Feir instability: Numerical solutions of the third-order model for ζ (—) compared with fully nonlinear solutions of the Euler equations ($\cdot\cdot\cdot$). The initial wave profile is given by (1.23).

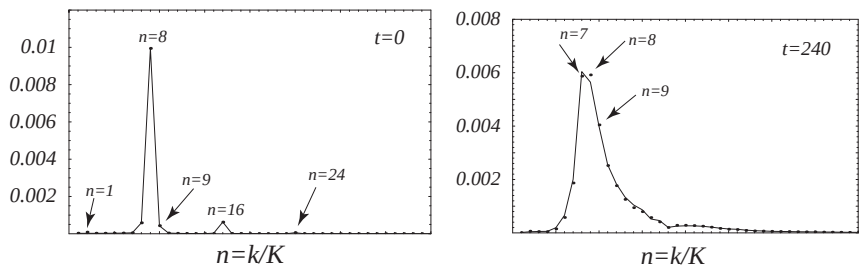

Fig. 1.3 Wavenumber spectra at $t = 0$ and $t = 240$ for the wave profiles shown in 1.2. Numerical solutions of the third-order model (—) are compared with exact solutions of the Euler equations $(\cdots)$.

equation serves as a reliable mathematical model for this situation, under the assumption that the wave spectrum remains narrow-banded. Based on our observation that the wave spectra become wide, a long-term prediction using the NLS model might be inaccurate for the evolution of a modulated wave envelope.

1.4 Numerical Solutions for Two-dimensional Waves

1.4.1 *Nonlinear resonant wave-wave interactions*

As originally demonstrated by Phillips (1960), three trains of gravity waves in deep water, with wave numbers $\boldsymbol{k}_1$, $\boldsymbol{k}_2$, and $\boldsymbol{k}_3$, are capable of interacting such that energy is transferred to a fourth wave number, $\boldsymbol{k}_4$. In order for this continuous energy exchange to occur, it is necessary that the following conditions be simultaneously satisfied:

$$\boldsymbol{k}_1 \pm \boldsymbol{k}_2 \pm \boldsymbol{k}_3 \pm \boldsymbol{k}_4 = 0, \quad \omega_1 \pm \omega_2 \pm \omega_3 \pm \omega_4 = 0, \tag{1.24}$$

where ${\omega_i}^2 = gk_i$ $(i = 1, 2, 3, 4)$ with $k_i = |\boldsymbol{k}_i|$.

For the special case in which two of the primary gravity trains coincide ($\boldsymbol{k}_1 = \boldsymbol{k}_3$), and are orthogonal to the third wave train (-$\boldsymbol{k}_2$), the resonant condition (1.24) between the primary wave trains and the resonant, or tertiary, wave (-$\boldsymbol{k}_4$) can be written as

$$2\boldsymbol{k}_1 - \boldsymbol{k}_2 - \boldsymbol{k}_4 = 0, \quad 2\omega_1 - \omega_2 - \omega_4 = 0, \tag{1.25}$$

and, from the dispersion relation between ω_4 and k_4, it must be true that

$$(2\omega_1 - \omega_2)^2 = g\sqrt{4{k_1}^2 + {k_2}^2} = \sqrt{4{\omega_1}^4 + {\omega_2}^4}. \tag{1.26}$$

Upon simplifying the equation with the substitution $r = \omega_1/\omega_2$, the only non-trivial solution is given (Longuet-Higgins 1962) by

$$r_c = \omega_1/\omega_2 = 1.7357, \quad k_1/k_2 = 3.0123. \tag{1.27}$$

For resonant conditions, Longuet-Higgins (1962) showed that tertiary wave amplitude will grow with time according to

$$k_4 a_4 = \frac{G}{2}(k_1 a_1)^2 (k_2 a_2)\, \omega_4\, t, \tag{1.28}$$

where G is a non-dimensional function of the angle between the two primary waves and the frequency ratio r and, for the case of mutually perpendicular primary waves, $G = 0.442$. From this equation, it is evident that the amplitude of the tertiary wave is expected to grow linearly with interaction time between the primary wave trains.

In order to verify this resonant mechanism, two experiments were carried out independently by Longuet-Higgins & Smith (1966) and McGoldrick *et al.* (1966) for two mutually-perpendicular wave trains. Both experiments confirmed the linear growth of resonant waves, but the measured growth rate of Longuet-Higgins & Smith was lower than the predicted value of Longuet-Higgins (1962), while the opposite trend was observed in the experiments of McGoldrick *et al.*

To numerically model the interaction of two intersecting wave trains, we initially superimpose two third-order progressive gravity waves, whose surface profile and velocity potential are given by

$$\zeta_i = a_i \left[\left(1 + \frac{1}{8}(k_i a_i)^2\right) \cos\theta_i + \frac{1}{2}(k_i a_i)\cos(2\theta_i) + \frac{3}{8}(k_i a_i)^2 \cos(3\theta_i) \right], \tag{1.29}$$

$$\Phi_i = a_i \sqrt{g/k_i}\, \mathrm{e}^{k_i \zeta_i} \sin\theta_i, \tag{1.30}$$

where $\theta_i = \boldsymbol{k}_i \cdot \boldsymbol{x}$ with $\boldsymbol{k}_1 = (k_1, 0)$ and $\boldsymbol{k}_2 = (0, k_2)$. In our numerical experiment, we solve the third-order equations given by (1.11)–(1.12) with $g = 1$, $\lambda_1 = 1$, $\lambda_2 = 3.0123$, $k_1 a_1 \simeq 0.094$, and $k_2 a_2 \simeq 0.085$. The number of the primary waves in each direction is equal to 4 and the number of Fourier modes used is $N = M = 128$.

As shown clearly in figure 1.4, the amplitude of the resonant wave in our numerical computation does grow linearly with time. As might be expected, the resonant wave amplitudes are closer to the theoretical values at smaller times. As time increases, the resonant wave continues to grow and eventually begins to interact with the two primary waves, rendering the theoretical prediction invalid. At the end of computation ($t \simeq 335$), the resonant wave is nearly 1/3 the amplitude of a_1, suggesting that a

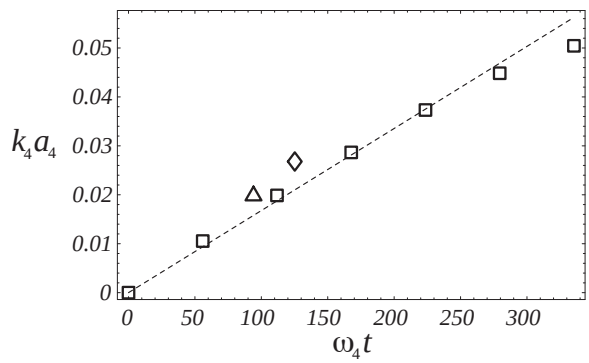

Fig. 1.4 Numerical solutions (□) for the growth of resonant wave (a_4) for $r(=\omega_1/\omega_2) = 1.7357$ compared with the theoretical prediction (- - -) by Longuet-Higgins (1962). For references, experimental data of McGoldrick *et al.* (1966) are shown for r=1.73 (△) and $r = 1.74$ (◇).

comparison of theoretical vs. numerical results beyond this time would have little significance. Compared with our numerical results, the growth rates measured by McGoldrick *et al.* (1966) are still higher and, currently, the origin of this discrepancy is not yet known. Notice that the frequency ratios for the earlier experiment and our computation are slightly different, but we have verified that this difference is not a source of discrepancy.

Table 1.1 Numerical results

$\omega_4 t$	k_1a_1	k_2a_2	k_4a_4
0	0.09425	0.08489	0
111.8	0.09362	0.08493	0.01987
223.6	0.09173	0.08497	0.03732
335.4	0.08954	0.08505	0.05044

As shown in table 1.1, another notable trend is that a_2 grows slowly as a_1 decays. This is an indication of an energy transfer from $\boldsymbol{k}_1$ to $\boldsymbol{k}_2$ accompanying the resonant interaction, as was noted by McGoldrick *et al.* (1966).

1.4.2 *Nonlinear evolution of random wave fields*

To examine the nonlinear evolution of a random wave field, an initial condition generated using the JONSWAP spectrum is considered. This simulation is similar to simulations carried out by Onorato, Osborne & Serio

(2002) who used an equation similar to the Zakharov equation.

The JONSWAP spectrum is given in terms of the wave frequency ω by

$$\mathrm{S}(\omega) = \frac{\alpha}{2\,k^4}\, e^{-1.25(\omega_p/\omega)^4}\gamma^{\exp\left(-\frac{(\omega-\omega_p)^2}{2\,\sigma^2\omega_p^2}\right)}, \tag{1.31}$$

where $k = \omega^2/g$, ω_p is the frequency of the dominant (principal) wave, α and γ are constants that shape the spectrum, and σ is a simple function of ω given by

$$\sigma = \begin{cases} \sigma_1 & \text{for } \omega \le \omega_p \\ \sigma_2 & \text{for } \omega > \omega_p \end{cases}. \tag{1.32}$$

To create a multi-directional wave spectrum, the JONSWAP spectrum $\mathrm{S}(\omega)$ given by (1.31) is multiplied by the following function for angular dependence:

$$\mathrm{H}(\theta) = \begin{cases} \frac{1}{\beta}\cos^2\left(\frac{\pi}{2\beta}\theta\right) & \text{for } -\beta \le \theta \le \beta \\ 0 & \text{otherwise} \end{cases}, \tag{1.33}$$

where θ represents the angle between the x-axis and the direction of wave propagation, and β is an angle specifying the maximum directional spread in the spectrum.

To generate an initial condition from the JONSWAP spectrum (1.31) with the directional spreading function (1.33), we first compute the wave frequency ω, at a given wave number k, using the linear deep-water dispersion relationship between ω and k, and the wave propagation direction θ for $1 \le n \le N$, $1 \le m \le M$:

$$k_{nm} = \sqrt{n{K_1}^2 + m{K_2}^2}, \quad \omega_{nm} = \sqrt{g\,k_{nm}}, \quad \theta_{nm} = \tan^{-1}(mK_2, nK_1), \tag{1.34}$$

where N and M are the numbers of Fourier modes in the x- and y-directions, respectively, and $K_1 = 2\pi/L_1$ and $K_2 = 2\pi/L_2$ with L_1 and L_2 being the computational domain lengths in the x- and y-directions, respectively, as defined in (1.13)–(1.14). From (1.31) and (1.33)–(1.34), one can find the Fourier coefficients for initial conditions for ζ and Φ in (1.13)–(1.14) as

$$a_{nm}(0) = \mathrm{A}_{nm}\, e^{i\delta_r}, \qquad b_{nm}(0) = i\mathrm{A}_{nm}\sqrt{\frac{g}{k_{nm}}}e^{i\delta_r}, \tag{1.35}$$

where δ_r is a random phase, and A_{nm} is defined by

$$\mathrm{A}_{nm} = \sqrt{2\,\mathrm{S}(\omega_{nm})\,\mathrm{H}(\theta_{nm})K_1K_2}\,. \tag{1.36}$$

The physical initial conditions for ζ and Φ are then found by taking the inverse fast Fourier transform of the Fourier coefficients described by (1.35).

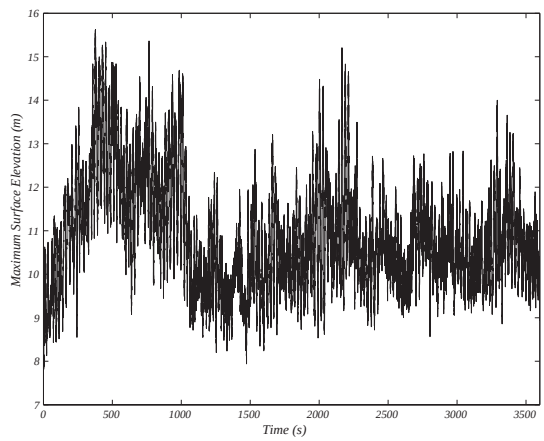

Fig. 1.5 Maximum wave elevation versus time for the multi-directional JONSWAP spectrum simulation.

Using the dimensional third-order equations given by (1.11)–(1.12), a simulation is carried out on a square domain with sides of length 2260 m, and the initial wave field obtained from (1.35) is allowed to evolve for one hour. Other physical parameters involved are $\rho = 1025\,kg/m^3$, $g = 9.81\,m/s^2$, $\lambda_p = 220\,m$ ($\omega_p = 0.529\,rad/s$), $\alpha = 0.015$ (significant wave height=9.5 m), $\gamma = 5.0$, $\sigma_1 = 0.07$, $\sigma_2 = 0.09$, and $\beta = 8°$. In this simulation, we use 256 Fourier modes for both the x- and y-directions, and 64 time steps per wave period of the peak wave.

Figure 1.5 shows the time evolution of the maximum wave elevation (elevation of the highest crest) observed inside the computational domain. One can see a peak in the maximum wave elevation (almost 1.7 times the significant wave height) occurring at approximately 378 seconds. Notice that relatively large amplitude waves can be observed over short initial periods for which nonlinear wave interactions are assumed to be active. As time increases, the maximum wave elevation decreases. A series of instantaneous free surface elevations are shown in figure 1.6, in which the localized nature of the large wave can be observed.

1.5 Discussion

We have presented a nonlinear formulation for surface waves in an infinitely deep fluid and have shown that the evolution of the free surface is governed by a pair of closed nonlinear evolution equations for two surface variables:

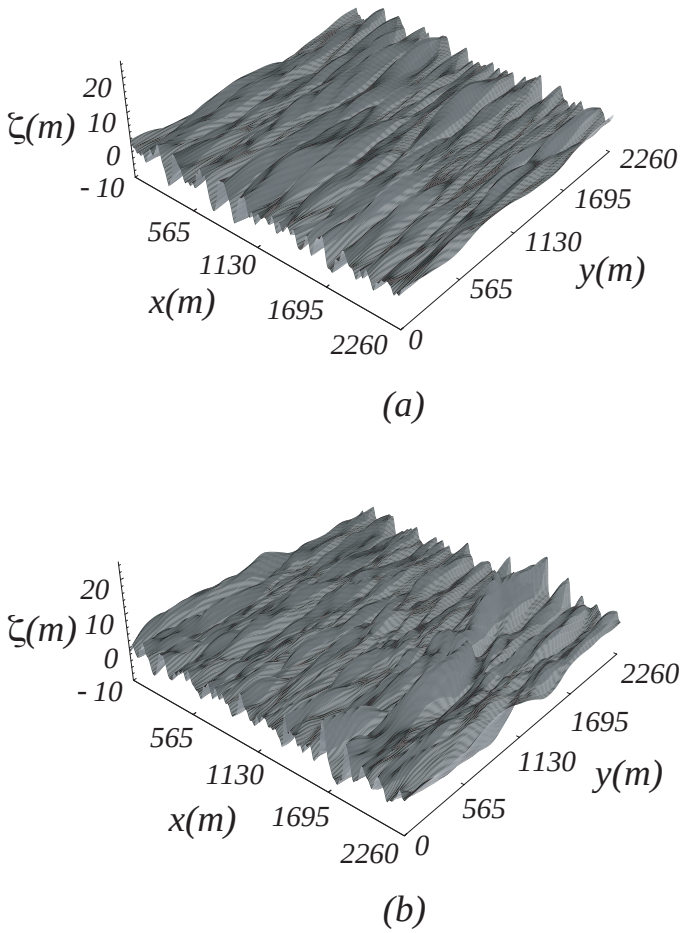

Fig. 1.6 Instantaneous surface elevation for the multidirectional JONSWAP spectrum simulation at (a) t=0 s, (b) t=378 s. The dominant direction of wave propagation is the positive x-direction.

the free surface elevation and the velocity potential at the free surface. The truncated form of the evolution equations correct up to third-order nonlinearity (or wave steepness) has been chosen for numerical experiments and solved using a pseudo-spectral method.

For validation of the truncated system, the one-dimensional solutions of the third-order equations have been compared with fully nonlinear solutions of a pair of exact evolution equations, derived from the two-dimensional

Euler equations, for progressive waves as well as for a wave train subject to sideband perturbations. Based on the fact that the third-order equations approximate surprisingly well the fully nonlinear Euler equations for one-dimensional waves, one can anticipate that the third-order equations serve as a reliable theoretical model even for two-dimensional waves, for which fully nonlinear solutions are difficult to obtain.

As a test of our numerical model for two-dimensional waves, we have examined nonlinear resonant wave interactions between two waves traveling in perpendicular directions. The numerical model describes the excitation of the initially absent resonant wave, as predicted by the theory of Phillips (1960) and Longuet-Higgins (1962). Initially, the resonant wave amplitude grows linearly with time, but the computed growth of the resonant wave eventually deviates from the theoretical prediction. In this paper, we have considered the simplest resonant wave interaction, but the numerical model should be equally applicable to more general nonlinear wave interactions. Numerical experiments for a wide range of wave slopes, frequency ratios, and propagation directions are currently underway.

Finally, we have simulated the generation of large amplitude waves in a random wave field, initialized by the JONSWAP spectrum multiplied by a directional spreading function, as a possible scenario of the occurrence of rogue waves. Our numerical solutions indeed have shown the creation of relatively short-lived local waves that are far larger than the background wave field. More systematic numerical experiments would help us better understand the physical mechanisms driving the creation of these intermittent large amplitude waves.

Bibliography

Benjamin, T. B. and Feir, J. E. (1967). The integration of wave trains on deep water. *J. Fluid Mech.* **27**, pp. 417–430.

Choi, W. (1995). Nonlinear evolution equations for two-dimensional waves in a fluid of finite depth. *J. Fluid Mech.* **295**, pp. 381–394.

Choi, W. and Camassa, R. (1999). Exact evolution equations for surface waves. *J. Eng. Mech.* **125**, pp. 756–760.

Choi, W. and Kent C. P. (2004). A pseudo-spectral method fir non-linear wave hydrodynamics, *Proceeding of the* 25th *Symposium on Naval Hydrodynamics* St. John's, Newfoundland.

Craig, W. and Sulem, C. (1993). Numerical simulation of gravity waves. *J. Comput. Phys.* **108**, pp. 73–83.

Dyachenko, A. L., Zakharov,V. E., and Kuznetsov, E. A. (1996). Nonlinear dynamics of the free surface of an ideal fluid, *Plasma Phys. Rep.* **22**, pp. 916–928.

Fenton ,J. D. and Rienecker, M. M. (1982). A Fourier method for solving nonlinear water-wave problems: application to solitary-wave interactions. *J. Fluid Mech.* **118**, pp. 411–443.

Fornberg, B. and Whitham, G. B. (1978). Numerical and Theoretical-Study of Certain Non-linear Wave Phenomena. *Phil. Trans. Royal Soc. A* **289**, pp. 373–404.

Hasselmann, K. (1962). On the nonlinear energy transfer in a gravity wave spectrum, Part 1. General theory. *J. Fluid Mech.* **12**, pp. 481-500.

Kent, C. P. and Choi, W. (2004). A hybrid asymptotic-numerical method for nonlinear surface waves. Part 1. Waves generated by a pressure forcing. Submitted for publication.

Lake, B. M., Yuen, H. C., Rungaldier, H. and Ferguson, W. E. (1977). Nonlinear deep water waves: theory and experiment. Part 2. Evolution of a continuous wave train. *J. Fluid Mech.* **83**, pp. 49–74.

Li, Y. A., Hyman, J. M. and Choi, W. (2004). A numerical study of the exact evolution equations for surface waves in water of finite depth. *Studies in Applied. Math.* **113**, pp. 303–324.

Longuet-Higgins, M. S. and Smith, N. D. (1966). An experiment on third-order

resonant wave interactions. *J. Fluid Mech.* **25**, pp. 417–435.

Longuet-Higgins, M. (1962). Resonant interactions between two trains of gravity waves. *J. Fluid Mech.* **12**, pp. 321–332.

Matsuno, Y. (1992). Nonlinear evolutions of surface gravity waves on fluid of finite depth. *Phys. Rev. Lett.* **69**, pp. 609–611.

McGoldrick, L. F., Phillips, O. M., Huang, N. E. and Hodgson, T. H. (1966). An experiment on third-order resonant wave interactions. *J. Fluid Mech.* **25**, pp. 417–435.

Onorato, M., Osborne, A. R., & Serio, M. (2002). Extreme wave events in directional, random oceanic sea states. *Physics of Fluids* **14**, pp. 25-28.

Ovsjannikov, L. V. (1974). To the shallow water theory foundation, *Arch. Mech.* **26**, pp. 407–422.

Phillips, O. M. (1960). On the dynamics of unsteady gravity waves of finite amplitude. Part 1. The elementary interactions. *J. Fluid Mech.* **9**, pp. 193–217.

Smith, R. A. (1998). An operator expansion formalism for nonlinear surface waves over variable depth. *J. Fluid Mech.* **363**, pp. 333–347.

West, B. J., Brueckner, K. A., Janda, R. S., Milder, D. M. and Milton, R. L. (1987). A New Numerical method for Surface Hydrodynamics. *J. Geophys. Res.* **92**, pp. 11803–11824.

Wu, T. Y. (1998). Nonlinear waves and solitons in water. *Physica D* **123**, pp. 48–63.

Wu, T. Y. (2001). A unified theory for modeling water waves. *Adv. Appl. Mech.* **37**, pp. 1-88.

Zakharov, V. E. (1968). Stability of periodic waves of finite amplitude on surface of a deep fluid. *J. Appl. Mech. Tech. Phys.* **9**, pp. 190–194.